Biatom Catalysts www.small-methods.cor

1 + 1' > 2: Heteronuclear Biatom Catalyst Outperforms Its Homonuclear Counterparts for CO Oxidation

Fengyu Li,* Xinying Liu, and Zhongfang Chen*

By means of density functional theory (DFT) computations, the CO/O_2 adsorption and CO oxidation pathways on the biatom catalyst, namely the heteronuclear $Fe_1Cu_1@C_2N$, in comparison with its homonuclear counterparts $Fe_2@C_2N$ and $Cu_2@C_2N$ are systemically investigated. The reactions of O_2 dissociation and CO oxidization with preadsorbed CO or O_2 are comparably studied. The computations find that the heteronuclear species $Fe_1Cu_1@C_2N$ possesses high stabilities and is feasible to be synthesized experimentally. More importantly, the heteronuclear $Fe_1Cu_1@C_2N$ catalyst has even better catalytic activity toward CO oxidation than its homonuclear counterparts, especially, without suffering the CO-poisoning problem CO-nosidering the myriad of unexplored heteronuclear dimers that can be potentially anchored at appropriate supports, this work opens a venue and provides a useful guideline for further developing CO-metal oased nanocatalysts.

1. Introduction

The oxidation of CO plays a very important role in reducing the environmental CO emission and removing CO contaminations from H₂-rich fuel gases for polymer electrolyte fuel cells (PEFC).^[1] Typically supported metal chances, especially those made of noble metals, e.g., Pt, Pd, Au, Ri., and Ru, exhibit high activity for CO oxidation. The cooperation between the support and the metal clusters can promote the O₂ activation and CO oxidation, for example, the activation barriers for O₂ discretion and CO oxidation on the TiO₂ supported Au and 1.1 ch sters are very low (nearly barrierless).^[2-4] However, the contactivities of the supported metal nanoparticles are size- and

Prof. F. Li
School of Physical Science and Technology
Inner Mongolia University
Hohhot 010021, China
E-mail: fengyuli@imu.edu.cn
Prof. X. Liu
Institute for the Development of En. 10 for African Sustainability
University of South Africa
Johannesburg 1710, South Africa
Prof. Z. Chen
Department of Chemistry

Department of Chemical University of Puerto Vice

Rio Piedras Carrus San Juan, PR 00931, USA E-mail: zhongfang hen@gmail.com

The ORCID identification number(s) for the author(s) of this article can be found under https://doi.org/10.1002/smtd.201800480.

DOI: 10.1002/smtd.201800480

shape-dependent;^[5–7] moreover, the large-scale applications are restrained by the high costs and the limited storage of these metals on earth.

The recently developed single-atom catalysts (SACs)[8-18] are promising to reduce the metal usage in catalysis and enhance the catalytic efficiency. In SACs, isolated individual atoms are dispersed on, and/or coordinated with, the surface atoms of an appropriate support, which maximizes the metal atom efficiency. Since the first SAC, single Pt atoms on FeO_x, [8] was reported in 2011, various SACs with metal oxide supports have been successfully fabricated, such as single Au/Pt/Ir/Ni/Os atoms on FeO_x,^[19–25] Co₃O₄,^[26] CeO₂,^[27] Al₂O₃,^[28] and M O 29 surfaces. At the same time, the SA's could be accessed by thermal a or Lation of supported metal nanopar-

ticles^[30] and direct atoms emitting from bulk metals.^[31] These experimental cx₁:0 ations also inspired many theoretical efforts. For e.c.m₁'e, various FeO_x-supported single metal atom catalysts for CO oxidation were systemically investigated by means of the sity functional theory (DFT) computations.^[32,33]

B.s. de. metal-oxides, a variety of porous graphene-like materials have been used as the substrates to anchor metal attris/clusters for catalysis. For example, it has been experimentally demonstrated that single metal atoms (Pt, Pd, Ag, Ir, Au) embedded in g-C₃N₄ are highly active for the semihydrogenation of 1-hexyne^[34] and electrochemical synthesis of ammonia, theoretical studies suggested that single transition metal atoms anchored on C₂N could serve as low-cost but highly efficient catalysts for oxygen evolution reaction, CO oxidation, nitrogen reduction reaction, HCOOH dehydrogenation, and CO₂ electrochemical reduction, and the noble metal atoms anchored on graphyne are very promising for low-temperature CO oxidation.

Beyond SACs, biatom catalysts, in which metal dimers are anchored on an appropriate substrate, have recently emerged as extended family members. Experimentally Yan et al. synthesized the stable platinum dimers (but dominantly in the oxidized form of Pt₂O_x without Pt—Pt bond) on graphene using atomic layer deposition, and demonstrated that Pt₂ dimers exhibit higher activity toward hydrolytic dehydrogenation of ammonia borane than that of graphene supported Pt₁ single atoms and nanoparticles.^[42] Theoretically, Luo et al. predicted that the Pd dimer embedded in graphene can effectively and selectively catalyze formic acid dehydrogenation;^[43] Sun and co-workers proposed that Cu dimer on graphene or Mn dimer

www.advancedsciencenews.com www.small-methods.com

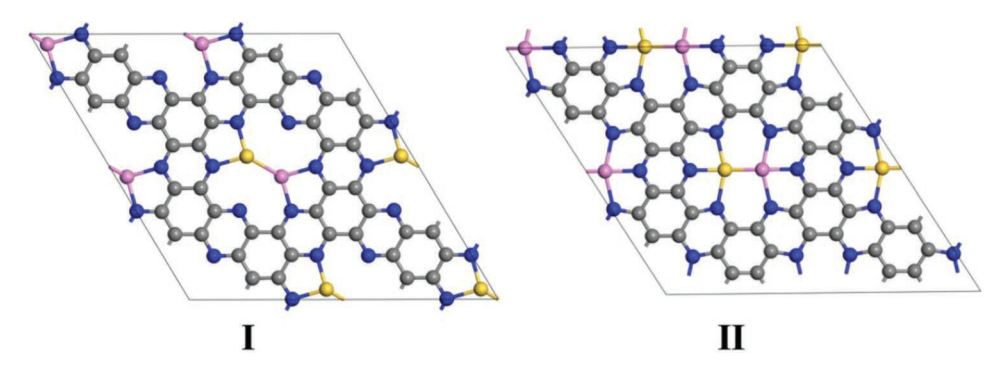


Figure 1. The two possible configurations of two metal atoms anchored C₂N (I and II). Color scheme: C, gray; N, blue; gold, M¹; pink, M².

on a phthalocyanine sheet exhibit higher catalytic activity for CO₂ reduction; [44–46] Compared with their single-atom counterparts, several double transition metal (TM) atoms supported by 2D crystal C₂N were predicted to have better catalytic performance for oxygen reduction reaction [47] and CO oxidation than their single-atom counterparts; [48] Several other transition metal dimers anchored on C₂N monolayers were also expected to exhibit high activity for some important chemical reactions, e.g., carbon dioxide electrochemical reduction (Cu₂@C₂N), [49] hydrogen evolution reaction (Co₂@C₂N, Ni₂@C₂N, Cu₂@C₂N, Ru₂@C₂N), [50] and nitrogen fixation (Mo₂@C₂N), [51] Mn₂@C₂N), [52]

Note that the metal dimers in the above mentioned biaton catalysts are all homonuclear. In principle, there are even non possibilities for heteronuclear dimers awaiting our property tions. In this work, by means of systematic DFT computations, we explored the potential of heteronuclear metal a mer le₁Cu₁ anchored on the porous C2N monolayer[53] as bi to a catalyst for CO oxidation, in comparison with its homo. 12 lear counterparts Fe₂@C₂N and Cu₂@C₂N. Our computational results demonstrated that the heteronuclear metal 4; as system Fe₁Cu₁@ C₂N has high stabilities and superior performance toward CO oxidation compared to the homonuclear counterparts, especially Fe₁Cu₁@C₂N does not suffer the CO-poisoning issue This work not only further spans the homonuclear bitter. catalysts to heteronuclear biatom catalysts, but also privides insights and guidelines to future experimental and con putational studies, and help promote the design and production of novel low-cost and efficient nanocatalysts.

2. Results and Discussion

2.1. Geometries and Thermodynami sabilities of the M¹M²@C₂N Monolayers (M¹/M² : C., or Fe)

Previous theoretical studie's showed that the single-atom catalyst $Fe_1@C_2N^{[54]}$ and binton, catalyst $Cu_2@C_2N$ possess good performance for CO ax dation. Thus, we constructed the homonuclear binton species $Fe_2@C_2N$ and the heteronuclear analogue Fe_1C_1 @ C_2N in this study.

We first examined the energetically most favorable anchoring site of Fe on the C_2N monolayer, for which three possible anchoring sites^[48] were considered. In the lowest energy configuration of Fe₁@ C_2N , the Fe atom forms three bonds with

N atoms, while for the case of $\operatorname{Cu_1@C_2N}$, the Cu atom prefers coordinating with two N atoms^[48] (Figure S1, Supporting Information). These results are in line with previous theoretical findings.^[50,54] For these two single metal atom complexes, Fe has the larger binding energy (E_b^{-1}) of 4.56 eV, Cu has the much smaller E_b^{-1} value of 3.25 eV.

For the biatom catalysts examined in this study (homonuclear: Fe₂@ C₂N and Cu₂@C₂N; heteronuclear: Fe₁Cu₁@C₂N), we only considered two configurations (I and II in Figure 1), in which two metal atoms are located in the porous region of C_{213} , since the binding energies at other sites are less favorable.[37,48,50] Both homo- and heteronuclear metal dimers prefer adopting Configuration U, in which two metal atoms coordinate with three N (101)'s of the C₂N substrate (Figure 1; Table S1, Supporting information). The distance between the two metal atoms in II is slightly longer than that in Configuration I (Table St) he three examined biatom catalysts. The binding energies of the second metal atoms (E_b^2) in biatom catalysts, 2.69, 4.31, and 2.48/3.79 eV for Cu2, Fe2, and Cu1Fe1@ C₂N mone avers, are slightly lower than the binding energies in the consession single-atom catalysts (E_b^{-1}) (3.25 and 4.56 eV for CL @C2N and Fe1@C2N, respectively). The preference of of guration II is accompanied by the more charge transfer between the metal atoms and the C₂N substrate (Table S1, Supporting Information). These highly favorable binding energies indicate the good thermodynamic stabilities of these biatom catalysts under investigation. Note that the Bader charge of Cu/Fe in the dimer M¹M²@C₂N of II configuration is smaller than monomer Cu₁@C₂N or Fe₁@C₂N, except that the value of Fe in $Fe_1Cu_1@C_2N$ (+1.10 |e|) is larger than that of $Fe_1@C_2N$ (+1.02 |e|), which could be assigned to electron transfer from Fe to Cu in the $Fe_1Cu_1@C_2N$, since 0.18 |e| charge transfer was found in the isolated Fe₁Cu₁ dimer from our calculations.

Note that the aggregation to metal atoms to larger clusters is a big concern. [40] To examine the resistance of the biatom species $M^1M^2@C_2N$ against aggregation into trimer or larger metal clusters, we compared the relative stability of the biatom species and the single-triatom systems using a $2 \times 1 \times 1$ supercell. For the homonuclear case, biatom species Cu_2 — Cu_2 and Fe_2 — Fe_2 are lower in energy than their single-triatom counterparts (Cu_1 — Cu_3 and Fe_1 — Fe_3) by 2.46 and 3.18 eV, respectively (Figure S2, Supporting Information). For the heteronuclear $Fe_1Cu_1@C_2N$ (in the form of Fe_1Cu_1 — Fe_1Cu_1 in $2 \times 1 \times 1$ supercell), its single-triatom counterparts could be the combination of Cu_1 and Cu_1Fe_2 (Cu_1 — Cu_1Fe_2) or Fe_1 and Fe_1Cu_2 (Fe_1 — Fe_1Cu_2); these



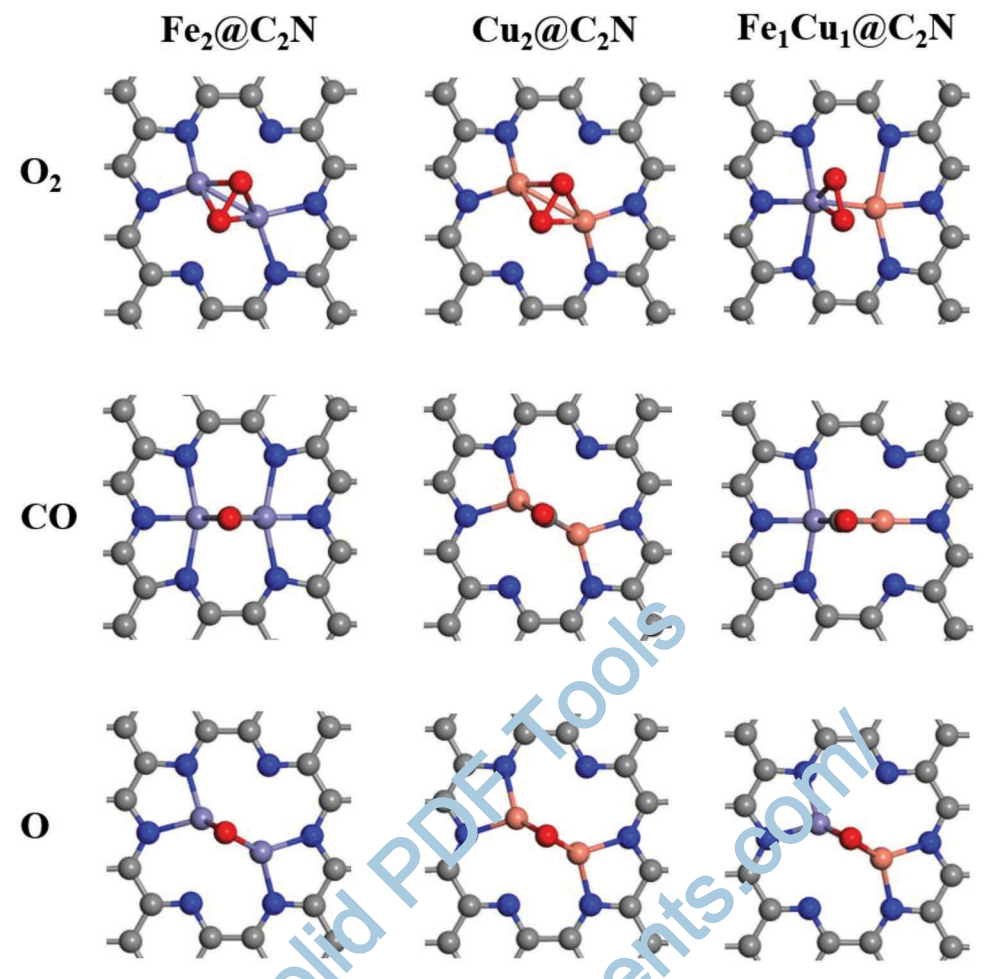


Figure 2. Top views of O_2 (top panel), CO (mildly panel) and O (bottom panel) ad C_2 on the three $M^1M^2@C_2N$ monolayers. Color scheme: C, gray; N, blue; purple, Fe; orange, Cu; red, O

two configurations are not only higher in energy than their corresponding biatom structures (by 0.51 and 0.95 eV, respectively), but also have rather high transition barriers (4.14 at d 3.98 eV, respectively) for their transition to biatom counterparts (Figure S2, Supporting Information). Thus, the Cu₁ to timers anchored on C_2N are expected to be stable without a gregation to larger clusters.

2.2. Adsorption of CO and O₂ on the CO₂N Monolayers

Before investigating the detailed reaction pathways of CO oxidation, we examined the a language of CO and O_2 molecules on the energetically most 'avorable configurations of the three $M^1M^2 @ C_2N$ monolayers.

Many adsorptions 'te' and configurations were considered, for example, four naturation sites of O_2 with side-on configuration were explored (Figure S3, Supporting Information): the O-O bond perpendicular to the metal bond (A), crossing to the metal bond (B), unilateral to the metal bond (C), and over the metal bond (C'). For the homonuclear $Fe_2@C_2N$ and $Cu_2@C_2N$ monolayers, O_2 adsorption with Configuration A is energetically

plost favored, and the structure of substrate will change from II to I upon O₂ adsorption for both cases (Figure 2); in contrast, for the heteronuclear Fe₁Cu₁@C₂N, the adsorbed O₂ is close to the Fe atom instead of over the metal bond center due to the much stronger interaction between Fe and O2, which can be reflected by the more enhanced O2 adsorption energy on $Fe_1 @ C_2 N$ ($E_{ad} = 2.41 eV$) than that on $Cu_1 @ C_2 N$ ($E_{ad} = 0.59 eV$) (Table S3, Supporting Information). Compared to the singlemetal-atom counterparts Fe₁@C₂N and Cu₁@C₂N, the O₂ adsorption strengths on homonulcear Fe₂@C₂N and Cu₂@ C₂N (2.62 and 1.33 eV, respectively) are enhanced (by 0.21 and 0.74 eV), and the O-O bond lengths are further elongated (by 0.05 and 0.17 Å, see Table 1 and Table S3, Supporting Information). When compared to the homonuclear counterparts (Table 1), the O₂ adsorption strength on heteronuclear Fe₁Cu₁@ C_2N ($E_{ad}=2.45$ eV) in between $Fe_2@C_2N$ ($E_{ad}=2.62$ eV) and $Cu_2@C_2N$ ($E_{ad} = 1.33 \text{ eV}$).

For CO adsorption, in the lowest energy structure, CO adopts an end-on configuration for all these three metal dimer systems, and only $\text{Cu}_2@\text{C}_2\text{N}$ will transform from configuration II to I upon CO adsorption (Figure 1). The CO adsorption strengths on the three biatom species are very comparable: the CO adsorption

www.advancedsciencenews.com



small methods

Table 1. The CO, O_2 , and O adsorption energies (E_{ad} , in eV) on $M^1M^2@C_2N$, their corresponding bond lengths (d_{C-O}/d_{O-O} , in Å), as well as the Bader charge (q, in |e|) of $CO/O_2/O$ and M^1/M^2 .

	Fe ₂ @C ₂ N	Cu ₂ @C ₂ N	Fe ₁ Cu ₁ @C ₂ N
$E_{ad}(O_2)$	2.62	1.33	2.45
d ₀₋₀	1.46	1.45	1.44
q (O ₂)	-1.08	-0.90	-0.92
9 (M)	+1.22 +1.30	+0.99 +0.99	+1.23 +0.77
E _{ad} (CO)	2.24	2.14	2.20
d _{C-O}	1.19	1.18	1.18
q (CO)	-0.66	-0.34	-0.50
q (M)	+1.18 +1.18	+0.78 +0.75	+1.13 +0.70
E _{ad} (O)	3.32	1.82	2.72
q (O)	-1.10	-0.85	-0.97
q (M)	+1.28 +1.35	+0.86 +0.87	+1.36 +0.85

energy on Fe₁Cu₁@C₂N ($E_{ad} = 2.20 \text{ eV}$) is between the values on Fe₂@C₂N ($E_{ad} = 2.24 \text{ eV}$) and Cu₂@C₂N ($E_{ad} = 2.14 \text{ eV}$).

Interestingly, the O_2/CO adsorption strength well correlates with the amount of charge transfer from the metal dimers to the adsorbate (Table 1; Table S3, Supporting Information): the more charge transfer from the metal dimers to the O_1/CO the stronger adsorption strength of O_2/CO . Notably a septou O_2/CO , both O_1/CO and O_2/CO and O_2/CO has larger adsorption energies of O_2 than those of O_2/CO . The pre-grable O_2 adsorption over O_2/CO is beneficial to these two callysts for excluding the O_2/CO poisoning issue.

Jiang and co-workers' very recent theoretical studies revealed that spin transition of single 12 atom could be induced by CO adsorption.^[55] Thus, we examined the magnetic configurations of the bare Fe₁Cu₁@C₂N and with 1-4 CO adsorption in a $2 \times 1 \times 1$ supercell using the DFT + U method (U = 4 eV for the d electrons of Fe and C atoms). The bare Fe₁Cu₁@C₂N is ferromagnetic with the magnetic moment of 7.36 μ_B , of which Fe atoms constitute dominantly (Figure S4a, Supporting Information, V.:1. One CO adsorption, the ferromagnetism of the Fe₁Cu & C₂N will not change (Figure S4b, Supporting Information), but the magnetic moment is reduced to be 4.74 $\mu_{\rm p}$. However, two CO adsorption on the Fe₁Cu₁@C₂N in either the symmetric (Figure S4c, Supporting Information, the magnetic moment: $0.00 \mu_{\rm B}$) or the asymmetric configuration (Figure S4d, Supporting Information, the magne ic moment: 2.91 $\mu_{\rm B}$) induces the spin transition from Commagnetism to antiferromagnetism. The antiferromagnetism remains with more (three and four) CO adsorption and the magnetic moments are 0.85 and 0.00 $\mu_{\rm B}$ is partively (Figure S4e,f, Supporting Information). Note that the energy differences between the spin configuration of antiferromagnetism and ferromagnetism are all less than 0.01 eV for the considered systems of the Fe₁Cu₁@C₂N with 0-4 CO molecules. The magnetic moment of each metal atom with 0-4 CO adsorption was listed in Table S4 (Supporting Information).

2.3. Mechanisms of CO Oxidation on the $M^1M^2@C_2N$ Monolayers

Since both O_2 and CO can be adsorbed on the $M^1M^2@C_2N$ monolayers with reasonable strength, we considered two possible conditions, the catalyst is preadsorbed by either O_2 or CO, when investigating CO oxidation on these biatom catalysts.

2.3.1. CO Oxidation on the O₂-Preadsorbed Catalyst Surface

We first examined the O_2 dissociation reactions on the three $M^1M^2@C_2N$ monolayers by taking the lowest-energy configurations of O_2 adsorbed $M^1M^2@C_2N$ monolayers as the initial structures. Our previous study revealed that the O_2 dissociation on the $Cu_2@C_2N$ is endothermic by 0.27 eV, and the corresponding reaction barrier is 0.50 eV.^[48] However, the O_2 dissociations on $Fe_2@C_2N$ and $Fe_1Cu_1@C_2N$ monolayers are both barrierlessly, and exothermic by 1.48 and 1.56 eV, respectively (Figure S5, Supporting Information). These findings are reminiscent of the extremely low O_2 dissociation barriers on the C_2N monolayer supported transition metal dimers $(Co_2, Ni_3$ at $1 Cu_2$).^[47]

Countering preferable adsorption of O_2 over CO (except $C_1 \otimes C_2 N$) and the low barriers of O_2 dissociation on these bimetal systems, we started the CO oxidation over $Fe_2 \otimes C_2 N$, and $Fe_1 Cu_1 \otimes C_2 N$ monolayes with preadsorbed and dissociated O_2 . In this process, CO will react with the dissociated O atoms on the catalyst surface, followed by the regeneration of the original catalyst surface. Providing that the first chemisorbed O could be removed by the first CO easily, the removal of the second the misorbed O will be crucial for the recovery of the prioring biatom catalysts. Therefore, we first evaluated the feasiblish of removing the second atomic O on the metal dime is

recording to the Sabatier principle, [56] a moderate adsorption strength between the reactants and the catalyst is a key foltor for the catalytic performance. As shown in Table 1, the homonuclear $Fe_2@C_2N$ ($E_{ad}=3.32$ eV) and $Cu_2@C_2N$ ($E_{ad}=1.82$ eV) monolayers have the largest and smallest adsorption energy of the atomic O species, respectively; compared with their homonuclear analogs, the O adsorption energy on the heteronuclear $Fe_1Cu_1@C_2N$ catalyst ($E_{ad}=2.72$ eV) is between $Fe_2@C_2N$ (3.32 eV) and $Cu_2@C_2N$ (1.82 eV). These data suggest that the heteronuclear complex $Fe_1Cu_1@C_2N$ might outperform the homonuclear counterparts for the removal of the second atomic O.

We then computed the reaction energies and activation barriers of the CO oxidation by the second atomic O on these metal dimers. This process is expected to proceed via the Eley–Rideal (E–R) mechanism, in which the reactant CO directly reacts with the O atom from the gas phase passing a transition state, and the CO_2 product is released. On $Fe_1Cu_1@C_2N$, the reaction energy is -0.16 eV and the barrier of removing the second atomic O to form the second CO_2 is 0.69 eV (Figure 3). As we reported before, on $Cu_2@C_2N$, the removal of O by CO via E–R mechanism to form the second CO_2 is kinetically more favorable (with an activation barrier of 0.29 eV) and this E–R reaction step is exothermic (1.28 eV). [48]

www.small-methods.com

www.advancedsciencenews.com

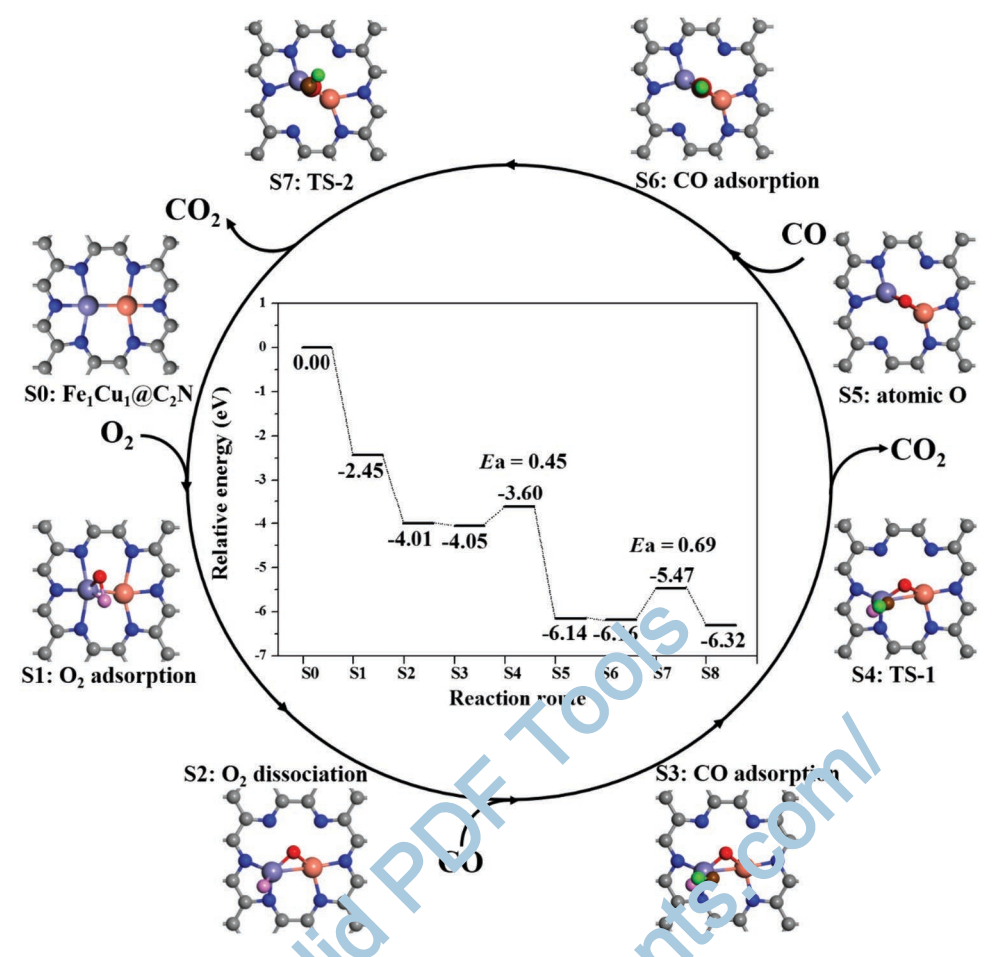


Figure 3. The reaction pathways (E–R) and energy pro, le for CO oxidation on the heteror x-le x-Fe $_1$ Cu $_1$ @C $_2$ N monolayer. The corresponding side views were given in Figure S7 (Supporting Information) Co or scheme: N, blue; Fe, purple C x-c ange; C in C $_2$ N, gray; C in CO, brown; O in CO, green; O in O $_2$, pink (first removed by CO) and red (second removed by CO).

However, the E–R process is slightly endothermic on $Fe_2@C_2N$ (0.05 eV), and the reaction barrier is as high at 1.53 eV. As expected by the Sabatier principle, the reaction barrier of removing O from the catalyst surface and the atomic D adsorption energy have a quasilinear relationship (Figure S6, Supporting Information). The overwhelming strong Condition and the difficulty in removing the atomic D on the $Fe_2@C_2N$ surface rule out its capacity to consider the strongly bound atomic O will block the catalytically active sites. Previous studies already confirmed the activity of $Cu_2@C_2N$ toward CO oxidation, [48] $t^2 = v_0$ we will not further discuss it in the following sections.

The above analyses showed that Leteronuclear $Fe_1Cu_1@C_2N$ can well catalyze the CO o.i.l. on by the second atomic O, as indicated by the small reaction barrier and the exothermic process of removing the comic O from the catalyst surface. Then, we checked if the CC or idation with the first atomic O is also facile on $Fe_1Cu_1@C_2N$. Excitingly, our computations revealed that this reaction is exothermic by 2.09 eV via overcoming a barrier of 0.45 eV.

Figure 3 (Figure S7, Supporting Information) illustrates the reaction profile of O_2 adsorption, dissociation, and CO oxidation on the $Fe_1Cu_1@C_2N$. Starting from the clean $Fe_1Cu_1@C_2N$

with the most stable configuration II, the O_2 molecule is alsorbed (S1) on the Fe atom, and then dissociates spontaneously (S2) to form an atomic O only attached to Fe and another O atom bridging Fe and Cu atoms. Subsequently, the singly bonded O atom will be approached by the first CO (S3), by passing over the transition state (S4) with the activation energy (E_a) of 0.45 eV, the first CO₂ molecule is produced companying with the reaction energy of 2.09 eV released. With the first CO2 released, only the second atomic O is bridge-bonded with Fe and Cu atoms (\$5). When the second CO approaches to the bridged O (S6), by passing over the transition state (S7) with the activation energy of 0.69 eV, the second CO₂ is formed (S8) with the exothermicity of 0.16 eV. Thus, the heteronuclear Fe₁Cu₁@C₂N exhibits good performance for CO oxidation on the O₂-preadsorbed catalyst surface among the examined dimer systems.

2.3.2. CO Oxidation on the CO-Preadsorbed Catalyst Surface

We then examined the CO oxidation over the CO preadsorbed $Fe_1Cu_1@C_2N$ following the bimolecular Langmuir–Hinshelwood (BLH) mechanism. As mentioned before, the

www.advancedsciencenews.com www.small-methods.com



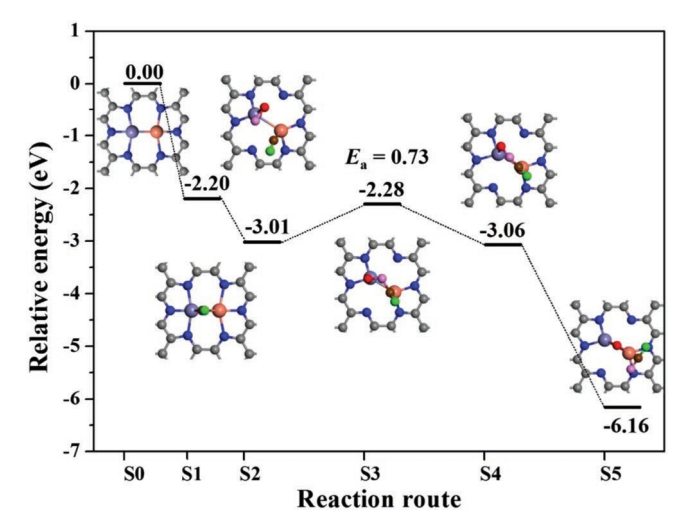


Figure 4. The reaction pathways (BLH) based on the coadsorption of CO and O_2 and energy profile for CO oxidation on the heteronuclear metal-dimer $Fe_1Cu_1@C_2N$ monolayer. The corresponding side views were given in Figure S8 (Supporting Information). Color scheme: N, blue; Fe, purple; Cu, orange; C in C_2N , gray; C in CO, brown; O in CO, green; O in O_2 , pink (reacted with CO) and red.

adsorption energy of CO on the Fe₁Cu₁@C₂N is 2.20 eV. Our computations showed that the O2-coadsorption is energetically favored by 0.81 eV. The coadsorbed O2 (O-O*) and CO (OC adopt side-on and end-on configurations (S2 in Figur. 4) respectively. The ability for the coadsorption of CO and O indicates the feasibility of the bimolecular L-H me banism. Figure 4 presents the reaction pathway and energy profile for CO oxidation following L-H mechanism, and Figure S8 (Supporting Information) gives the side views and k y geometric parameters of intermediates. Following this in achanism, first OC* approaches to O-O*, passing o re the transition state (\$3 in Figure 4, the intermolecular C···O Listance of 2.33 Å in S2 becomes to 1.50 Å in S3) with a barrier of 0.73 eV to form the intermediate OOCO* (\$4 in Figure 4). For the intermediate S4, the O-O and C-O bonds are elongated to be 1.46 and 1.22 Å, respectively, and the newly formed intermolecula. C-1) bond is 1.37 Å. Then, a CO₂ molecule is produced bar ie. le. sly (S5 in Figure 4, the OO distance is 3.00 Å) accompanied by a release of 3.10 eV of energy (Figure 4; Figure 50, Supporting Information).

Furthermore, we studied the situation with two CO molecules preadsorbed on the $Fe_1Cu_1@C_2N$, which can occur under high concentration of CO. To well situates such a condition, we explored the trimolecular ER (\mathbb{C}^{\bullet}) mechanism proposed by Li and co-workers when investigating the CO oxidation over the single Au atom support \mathbb{C}^{\bullet} is and N doped single-walled carbon nanotube, \mathbb{C}^{57} where \mathbb{C}_2 reacts with two adsorbed CO. On $Fe_1Cu_1@C_2N$, the adsorption energy of the second CO (1.00 eV) is lower than he individual CO adsorption energy (i.e., 2.20 eV for u.e. ins. CO), thus the CO coadsorption will be in compete on with the adsorption of two individual CO molecules. Both adsorbed CO (OC*) adopt the end-on configuration with the intermolecular \mathbb{C} C distance of 2.30 Å, and the coadsorption energy is 3.20 eV (S1 in Figure 5). Following TER mechanism, the reaction starts with the two adsorbed

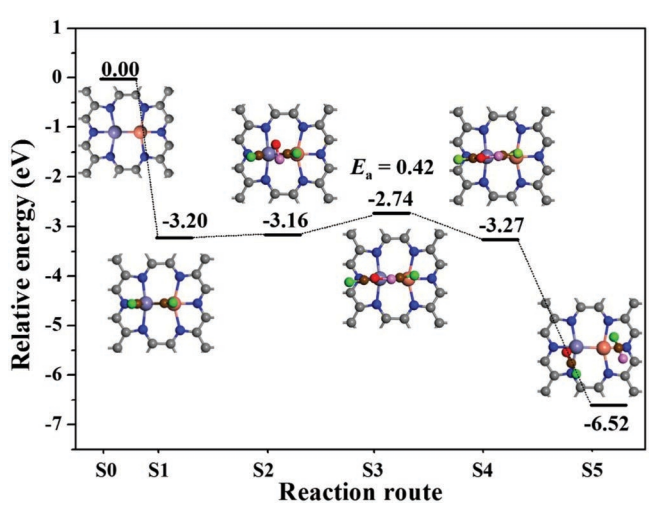


Figure 5. The reaction pathways based on the TER mechanism and the energy profile on the heteronuclear metal-dimer $Fe_1Cu_1@C_2N$ monolayer. The corresponding side views were given in Figure S9 (Supporting Information). Color scheme: N, blue; Fe, purple; Cu, orange; C in C_2N , gray; C in CO, brow. On CO, green; O in O_2 , pink and red.

CO (DC) and an O₂ approaching to the two adsorbed CO (S) in Figure 5), and the O₂ is activated by the two adsorbed CO instead of the Fe₁Cu₁ dim r. In the transition state S3 (Figure S9, Supporting Info motion), the O—O bond is elongated to 1.34 Å, and the distances between the two O atoms and the two C atoms (1 CC) are 1.78 and 1.97 Å, respectively. The activation barrier (0.42 eV) is significantly lower than that of the BLH motion sm (0.73 eV). Surpassing the transition state S3, a restagonal ring intermediate OCOOCO (S4 in Figure 5), O 1. eV lower in energy than S2, is formed, in which the O—O for id is further stretched to 1.46 Å, and the two newl formed C—O bonds are 1.36 and 1.38 Å, respectively. Then, the intermediate S4 dissociates into two CO₂ molecules (S. in Figure 5) spontaneously, and at the same time, 3.25 eV of heat is released.

To sum up, we examined the CO oxidation on Fe₁Cu₁@ C₂N monolayer following three different mechanisms, namely ER mechanism with O2-preadsorbed catalyst surface, BLH mechanism with CO-preadsorbed catalyst surface (low CO partial pressure), and TER mechanism with two CO molecules preadsorbed on catalyst surface (high CO partial pressure). Comparing the E-R, BLH, and TER routes discussed above, we could easily find the TER mechanism is the most favored pathway, since it has the lowest activation energy of 0.42 eV, thus it is recommended to perform CO oxidation at high CO partial pressure since it will favor TER mechanism. Notably, the largest activation energies of all the examined mechanisms (TER: 0.42 eV; ER: 0.69 eV; BLH: 0.73 eV) are less than 0.8 eV, indicating that the CO oxidation process could occur at room temperature.^[58] Interestingly, the notorious CO-poisoning problem could be avoided on Fe₁Cu₁@C₂N: O₂ and CO have comparable adsorption strengths (2.45 and 2.20 eV, respectively) on the catalyst surface, and O2 could react with the preadsorbed CO by surpassing moderate barriers (0.73 and 0.42 eV for the preadsorption of one and two CO, respectively). Thus, the hetero-nuclear Fe₁Cu₁@C₂N is quite promising as

www.advancedsciencenews.com

small

low-cost catalyst for CO oxidation at room temperature without suffering the CO-poising problem.

Notably, the heteronuclear $Fe_1Cu_1@C_2N$ outperforms its homonuclear counterparts ($Fe_2@C_2N$ and $Cu_2@C_2N$) as a catalyst for low-temperature CO oxidation: it is much easier to remove the chemisorbed atomic O on the $Fe_1Cu_1@C_2N$ than the $Fe_2@C_2N$ (reaction barrier 0.69 eV vs 1.53 eV); the O_2 dissociation on the $Fe_1Cu_1@C_2N$ is barrierlessly, while a barrier of 0.50 eV should be surpassed on the $Cu_2@C_2N$; [48] CO-poisoning will not be the limited issue for the $Fe_1Cu_1@C_2N$, but $Cu_2@C_2N$ is prone to be poisoned by CO molecules due to the higher CO adsorption energy compared with that of O_2 (2.14 eV vs 1.33 eV).

2.4. Origin of the Superior Catalytic Performance of Fe₁Cu₁@C₂N

To understand the much enhanced catalytic performance of Fe₁Cu₁@C₂N over its homonuclear counterparts (Fe₂@C₂N and $Cu_2 \otimes C_2 N$), we examined the density of states of the d electrons and analyzed the d-band centers of these three dimer species (Figure S10, Supporting Information). According to the d-band center theory, the position of the d-band center can differentiate the adsorption strength with adsorbates. Checking the relationship between the d-band centers, including the d-band centers of the spin-up channel (d-up) and spin down channel (d-down) and the adsorption energies of CO, O2, and O (Figure (we found that the adsorption energy change well correlates with the d-band center position: the adsorption straight of $CO/O_2/O$ on the $Fe_1Cu_1@C_2N$ is between them on 'b. $Fe_2@$ C₂N and Cu₂@C₂N, and the d-band center € spin-down channel for the Fe₁Cu₁@C₂N is placed between the d-down of the Fe₂@C₂N and Cu₂@C₂N. Thus, the de e. dence of the adsorption strength and the d-band center is in line with the d-band center theory proposed by Han man and Nørskov. [59]

We also noted that the $CO/O_2/O$ adsorption in the lowest-energy structures can induce the structural transformation of metal dimer from II to I, as shown in Figure 1. Thus, we further compared the d-band centers of the $Fe_1Cu_1@C_2$.

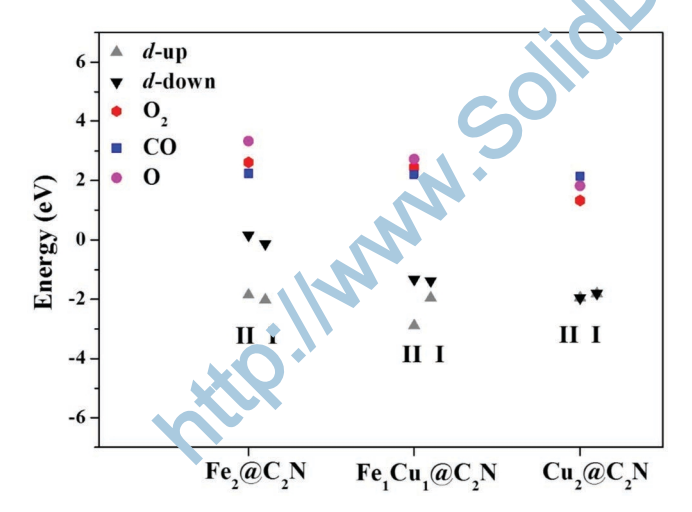


Figure 6. The d-band centers of configuration II and I, and the adsorption energies of CO, O_2 , and O for the $Fe_2@C_2N$, $Fe_1Cu_1@C_2N$ and $Cu_2@C_2N$.

different configurations with those of Fe $_2$ @C $_2$ N and Cu $_2$ @C $_2$ N. For Fe $_1$ Cu $_1$ @C $_2$ N, in either configuration I or II, the d-band centers of the spin-down channel are located between the corresponding values of Fe $_2$ @C $_2$ N and Cu $_2$ @C $_2$ N (Figure S10, Supporting Information and Figure 6); while the spin-down channel of the d-band centers of Fe $_2$ @C $_2$ N in both I and II configurations are quite close to the Fermi level, leading to the strong interaction with the adsorbates (CO, O $_2$, and O) and the concomitant high activation energy to remove the atomic O (as high as 1.53 eV). The cooperation of Fe and Cu endows the Fe $_1$ Cu $_1$ @C $_2$ N possessing the moderate d-band centers in configurations I and II, and thus leads to the heteronuclear species outperforming its homonuclear counterparts, consisting with previous theoretical results that catalysts with moderate d-band centers exhibit good catalytic performance. [58–61]

2.5. The Feasibility for Experimental Realization of Fe₁Cu₁@C₂N

So far single metal atom on C₂N has not been synthesized yet, instead the Pa nanoparticles dispersed within the nitrogenated holes of $C_2 N^{-2}$ and Fe nanoparticles supported on $C_2 N^{[63]}$ were obtaine b Baek and co-workers. Previously we proposed a synthetic route and simulated the synthesis process for experin ental realization of Cu₁@C₂N and Cu₂@C₂N using CuCl₂ as the metal precursor, and found that both catalysts are quite easy to be obtained. [48] Since the E_b value of Fe (3.79 eV) is much larger than that of Cu (2.6) eV) for Fe₁Cu₁@C₂N (Table S1, Supporting Information) we then examined the feasibility for experimental realization of Fe₁Cu₁@C₂N based on Cu₁@C₂N and FeCl₂ by computing the energy profile of the proposed synthetic rome (Figure S11, Supporting Information) and simulating the synthesis process by first principles molecular dynamics (F)MD) at 350 K in an NVT canonical ensemble. All the extron steps can easily occur since they are either spontal. 20 is (barrierless) or only slightly endothermic (Figure S12, Supporting Information). In our FPMD simulations, the FeCl₂ the solution is observed to adsorb on the Cu₁@C₂N, afterward the Cl⁻ ions is desorbed. Within 0.5 ps, Fe₁Cu₁@C₂N is formed (Figure S13, Supporting Information). The FPMD simulation (5 ps at 800 K) revealed that the Fe₁Cu₁@C₂N system has very good thermal stability (Figure S14, Supporting Information). Note that during the period of revision, the Cu_1^0 – Cu_1^{x+} pair anchored on Pd₁₀Te₃ alloy nanowires have been developed for selective and efficient electrochemical reduction of CO₂ [64] the Zn-Co atomic pairs on N-doped carbon support was experimentally achieved and the high activity toward oxygen reduction reaction was demonstrated.^[65] Thus, we believe that the highly stable and efficient Fe₁Cu₁@C₂N catalysts could be synthesized by using CuCl₂ and FeCl₂ as the metal precursors.

3. Conclusions

In summary, by means of DFT computations, we explored the potential of using C_2N monolayer to anchor heteronuclear metal dimer, i.e., $Fe_1Cu_1@C_2N$, as the biatom catalyst for CO oxidation, in comparison with its the homonuclear counterparts $Fe_2@C_2N$ and $Cu_2@C_2N$. The heteronuclear $Fe_1Cu_1@C_2N$

www.advancedsciencenews.com

www.small-methods.com

small __ methods

has good thermodynamic and thermal stabilities, and exhibits superior performance toward CO oxidation compared to the homonuclear catalysts $Fe_2@C_2N$ and $Cu_2@C_2N$, and especially does not suffer the notorious CO oxidation problem. The heteronuclear $Fe_1Cu_1@C_2N$ species is feasible to be synthesized according to our proposed synthetic route and MD simulations. Our comparative study suggests that the heteronuclear biatom catalyst, namely the iron copper dimer anchored on suitable substrate, is highly active for CO oxidation.

Heteronuclear dimers provide a simple means of modulating the d-band centers, so that the optimal interactions with the intermediates can be achieved, thus enhancing the catalytic performance. Note that this work is the first attempt to investigate heteronuclear biatom catalysts, and there might be some metal dimers exhibiting even better performance than $Fe_1Cu_1@C_2N$ for CO oxidation, considering the vast number of possible combinations of heteronuclear dimers. This work not only spans the single-atom catalysts, but also provides useful insights and guidelines to future theoretical and experimental investigations, and help promote the design and development of novel low-cost and efficient nanocatalysts for many other important reactions.

4. Computational Details

Our spin-polarized DFT computations were based on the generalized gradient approximation (GGA) in the form of the Perdew-Burke-Ernzerhof exchange-correlation functional (PBE). [66] Frozen-core all-electron projector augmented vave (PAW) method^[67] was used as implemented in the Jienna ab initio simulation package (VASP). [68] The Monthors -Pack scheme^[69] of $(5 \times 5 \times 1)$ k-points mesh was up lies to carry out the numerical integrations in the reciprocal space. The kinetic energy cutoff for the plane-wave basis set was chosen to be 500 eV. The optimized lattice parameter of the 2D C₂N unit cell (C₁₂N₆) is 8.33 Å, which agrees well with both experimental value^[53] and previous theoretical results.^[37] The computations on the isolated molecules and atoms were carried out in a (10 Å \times 10 Å \times 10 Å) unit cell with the Γ -point and for the k-point sampling. The reaction pathways were havest gated by using the climbing image nudged elastic band method (CI-NEB),^[70] and for each reaction, 5–9 images was accepted between the reactant and the product. Bader change analysis [71] was used to evaluate the charge transfer. Unless cated otherwise, the unit cell was used in our computations

The binding energy (E_b) of a metal at m or the adsorption energy (E_{ad}) of an adsorbate (O_2, CO, CC) on the substrate was defined as $E_b/E_{ad} = E + E' - E_{tot}$, where E, E', and E_{tot} represent the total energies of the clean slatent energies at the slab after all reprion, respectively. In the case of the coadsorption of two perios A and B, E' is the sum of the total energies of isolated A and B. According to this definition, a positive (negative) value of E_b/E_{ad} indicates that the adsorption is exothermic (and othermic).

Supporting Information

Supporting Information is available from the Wiley Online Library or from the author.

Acknowledgements

This work was supported in China by the National Natural Science Foundation of China (No. 11704203) and the Startup Project of Inner Mongolia University in China, and in USA by NSF-CREST Center for Innovation, Research and Education in Environmental Nanotechnology (CIRE2N) (Grant Number HRD-1736093). All the computations were performed on PARATEAR at Guangzhou Supercomputer Center.

Conflict of Interest

The authors declare no conflict of interest.

Keywords

biatom catalysis, CO oxidation, density functional calculations, heteronuclear, single-atom catalysis

Received: November 22, 2018 Revised: February 2, 2019 Published online:

- [1] K. Liu, A. Wang, T. Zhang, ACS Ca. al. 2012, 2, 1165.
- [2] L. M. Molina, M. D. Rasmuss in, 3. Hammer, J. Chem. Phys. 2004, 120, 7673.
- [3] L. Li, Y. Gao, H. Li, Y. Tha, Y. Pei, Z. Chen, X. C. Zeng, J. Am. Chem. Soc. 2013, 135 1955.
- [4] W. An, P. Liu, Phys. Chem. Phys. 2016, 18, 30899.
- [5] M. Haruta, N. G., da, T. Kobayashi, S. lijima, J. Catal. 1989, 115, 301.
- [6] K. Judai, A. A. Det, A. S. Wörz, U. Heiz, C. R. Henry, J. Am. Chem. Soc. 2 0 , 126, 2732.
- [7] T. Coralow, B. Brandt, D. E. Starr, M. S. Laurin, K. Shaikhutdinov, S. hauermann, J. Libuda, H.-J. Freund, *Angew. Chem., Int. Ed.* 10-6, 45, 3693.
- [8, 5. Qiao, A. Wang, X. Yang, L. F. Allard, Z. Jiang, Y. Cui, J. Liu, J. Li, T. Zhang, *Nat. Chem.* **2011**, *3*, 634.
- [9] X. Yang, A. Wang, B. Qiao, J. Li, J. Liu, T. Zhang, Acc. Chem. Res. 2013, 46, 1740.
- [10] W. Zhang, W. Zheng, Adv. Funct. Mater. 2016, 26, 2988.
- [11] J. Liu, ACS Catal. 2017, 7, 34.
- [12] B. Bayatsarmadi, Y. Zheng, A. Vasileff, S.-Z. Qiao, Small 2017, 13, 1700191.
- [13] L. Wang, L. Huang, F. Liang, S. Liu, Y. Wang, H. Zhang, Chin. J. Catal. 2017, 38, 1528.
- [14] F. Chen, X. Jiang, L. Zhang, R. Lang, B. Qiao, Chin. J. Catal. 2018, 39, 893.
- [15] C. Zhu, S. Fu, Q. Shi, D. Du, Y. Lin, Angew. Chem., Int. Ed. 2017, 56, 13944.
- [16] J.-C. Liu, Y. Tang, Y.-G. Wang, T. Zhang, J. Li, Natl. Sci. Rev. 2018, 5, 638
- [17] a) Z. Li, D. Wang, Y. Wu, Y. Li, Natl. Sci. Rev. 2018, 5, 673; b) J. Wang, Z. Li, Y. Wu, Y. Li, Adv. Mater. 2018, 30, 1801649.
- [18] L. Zhang, M. N. Banis, X. Sun, Natl. Sci. Rev. 2018, 5, 629.
- [19] J. Lin, A. Wang, B. Qiao, X. Liu, X. Yang, X. Wang, J. Liang, J. Li, J. Liu, T. Zhang, J. Am. Chem. Soc. 2013, 135, 15314.
- [20] J. Liang, J. Lin, X. Yang, A. Wang, B. Qiao, J. Liu, T. Zhang, J. Li, J. Phys. Chem. C 2014, 118, 21945.
- [21] H. Wei, X. Liu, A. Wang, L. Zhang, B. Qiao, X. Yang, Y. Huang, S. Miao, J. Liu, T. Zhang, Nat. Commun. 2014, 5, 5634.

www.advancedsciencenews.com www.small-methods.com

[22] B. Qiao, J. Liang, A. Wang, C. Xu, J. Li, T. Zhang, J. Liu, Nano Res. 2015, 8, 2913.

- [23] J. Lin, B. Qiao, N. Li, L. Li, X. Sun, J. Liu, X. Wang, T. Zhang, Chem. Commun. 2015, 51, 7911.
- [24] B. Qiao, J. X. Liang, A. Wang, J. Liu, T. Zhang, Chin. J. Catal. 2016, 37, 1580.
- [25] J. Liang, X. Yang, A. Wang, T. Zhang, J. Li, Catal. Sci. Technol. 2016, 6, 6886.
- [26] B. Qiao, J. Lin, A. Wang, Y. Chen, T. Zhang, J. Liu, Chin. J. Catal. 2015, 36, 1505.
- [27] B. Qiao, J. Liu, Y. Wang, Q. Lin, X. Liu, A. Wang, J. Li, T. Zhang, J. Liu, ACS Catal. 2015, 5, 6249.
- [28] M. Moses-DeBusk, M. Yoon, L. F. Allard, D. R. Mullins, Z. Wu, X. Yang, G. Veith, G. M. Stocks, C. K. Narula, J. Am. Chem. Soc. 2013, 135, 12634.
- [29] D. Yang, S. Zhang, P. Xu, N. D. Browning, D. A. Dixon, B. C. Gates, Chem. - Eur. J. 2017, 23, 2532.
- [30] J. Yang, Z. Qiu, C. Zhao, W. Wei, W. Chen, Z. Li, Y. Qu, J. Dong, J. Luo, Z. Li, Y. Wu, Angew. Chem., Int. Ed. 2018, 57, 14095.
- [31] Y. Qu, Z. Li, W. Chen, Y. Lin, T. Yuan, Z. Yang, C. Zhao, J. Wang, C. Zhao, X. Wang, F. Zhou, Z. Zhuang, Y. Wu, Y. Li, *Nat. Catal.* 2018, 1, 781.
- [32] F. Li, Y. Li, X. C. Zeng, Z. Chen, ACS Catal. 2015, 5, 544.
- [33] J. Liang, Q. Yu, X. Yang, T. Zhang, J. Li, Nano Res. 2018, 11, 1599.
- [34] a) G. Vilé, D. Albani, M. Nachtegaal, Z. Chen, D. Dontsova, M. Antonietti, N. López, J. Pérez-Ramírez, Angew. Chem., Int. Ed. 2015, 54, 11265; b) Z. Chen, S. Mitchell, E. Vorobyeva, R. K. Leary, R. Hauert, T. Furnival, Q. M. Ramasse, J. M. Thomas, P. A. Midgley, D. Dontsova, M. Antonietti, S. Pogodin, N. López, J. Pérez-Ramíre, Adv. Funct. Mater. 2017, 27, 1605785.
- [35] X. Wang, W. Wang, M. Qiao, G. Wu, W. Chen, T. Yuan, Q. X. M. Chen, Y. Zhang, X. Wang, J. Wang, J. Ge, X. Hong, Y .. 1. W., Y. Li, Sci. Bull. 2018, 63, 1246.
- [36] X. Li, P. Cui, W. Zhong, J. Li, X. Wang, Z. Wang, Jiang Chem. Commun. 2016, 52, 13233.
- [37] D. Ma, Q. Wang, X. Yan, X. Zhang, C. He, D. Z. o. I. Tang, Z. Lu, Z. Yang, Carbon 2016, 105, 463.
- [38] Z. Wang, Z. Yu, J. Zhao, Phys. Chem. Chem. Phys. 2018, 20, 12835.
- [39] W. Zhong, Y. Liu, M. Deng, Y. Zhang, C. Jia. J. V. Prezhdo, J. Yuan, J. Jiang, J. Mater. Chem. A 2018, 6, 11105.
- [40] X. Cui, W. An, X. Liu, H. Wang, Y. Men, J. Wang, Nanoscale 2018, 10, 15262.
- [41] D. Ma, T. Li, Q. Wang, G. Yang, C. He, B. Ma, Z. Lu, Carbo 295, 756.
- [42] H. Yan, Y. Lin, H. Wu, W. Zhang, Z. Sun, H. Cheng, W. Lir, C. Vang, J. Li, X. Huang, T. Yao, J. Yang, S. Wei, J. Lu, Nat. On viv. 2017, 8, 1070.
- [43] Q. Luo, W. Zhang, C.-F. Fu, J. Yang, Int. J. Hydroge, Energy 2018, 43,
- [44] Y. Li, H. Su, S. H. Chan, Q. Sun, ACS Catal. 2013, 5, 6658

- [45] G. Zhu, Y. Li, H. Zhu, H. Su, S. H. Chan, Q. Sun, Nano Res. 2017, 10, 1641.
- [46] H. Shen, Y. Li, Q. Sun, J. Phys. Chem. C 2017, 121, 3963.
- [47] X. Li, W. Zhong, P. Cui, J. Li, J. Jiang, J. Phys. Chem. Lett. 2016, 7, 1750.
- [48] F. Li, Z. Chen, Nanoscale 2018, 10, 15696.
- [49] J. Zhao, J. Zhao, F. Li, Z. Chen, J. Phys. Chem. C 2018, 122, 19712.
- [50] X. Zhang, A. Chen, Z. Zhang, M. Jiao, Z. Zhou, J. Mater. Chem. A 2018. 6, 11446.
- [51] X. Zhang, A. Chen, Z. Zhang, Z. Zhou, J. Mater. Chem. A 2018, 6, 18599.
- [52] Z. W. Chen, J.-M. Yan, Q. Jiang, Small Methods 2018, 2, 1800291.
- [53] J. Mahmood, E. K. Lee, M. Jung, D. Shin, I.-Y. Jeon, S.-M. Jung, H.-J. Choi, J.-M. Seo, S.-Y. Bae, S. D. Sohn, N. Park, J. H. Oh, H.-J. Shin, J.-B. Baek, *Nat. Commun.* 2015, 6, 6486.
- [54] B. L. He, J. S. Shen, Z. X. Tian, Phys. Chem. Chem. Phys. 2016, 18, 24261.
- [55] Q.-K. Li, X.-F. Li, G. Zhang, J. Jiang, J. Am. Chem. Soc. 2018, 140, 15149.
- [56] P. Sabatier, La Catalyse en Chimie Organique, Librairie Polytechnique, Paris et Liège 1920.
- [57] S. Ali, T. Liu, Z. Lian, B. Li, D. S. Su, J. Mater. Chem. A 2017, 5, 16653.
- [58] J. Liang L.Y., X. Yang, T. Zhang, J. Li, Nano Res. 2018, 11, 1599.
- [59] B. H'arr, n.r., J. K. Nørskov, Advances in Catalysis, Vol. 45, Academic P. S. C., San Diego, 2000, p. 71.
- [10] I. L., H. Shu, C. Hu, Z. Shi, X. Liu, P. Liang, X. Chen, ACS Appl. Mater. Interfaces 2015, 7, 27405.
- [61] G. Zhu, Y. Li, H. Zhu, H. Su, S. I. Chan, Q. Sun, ACS Catal. 2016, 6, 6294.
- [62] J. Mahmood, F. Li, C. Ki, n. H.-J. Choi, O. Gwon, S.-M. Jung, Jeong-MinSeo, S.-J. Tho, Y.-W. Ju, H. Y. Jeong, G. Kim, J.-B. Baek, Nat. Nanotechnol. 2011, 12, 441.
- [63] J. Mahmood, S.-J. S.-M. Jung, M. S. Okyay, I. Ahmad, S.-J. Kim, N. Park, H. Y. 2018, J.-B. Baek, *Nano Energy* **2018**, *44*, 304.
- [64] J. Jiao, R. Lin, S. Liu, W. C. Cheong, C. Zhang, Z. Chen, Y. Pan, J. Tar Y. K. Wu, S. F. Hung, H. M. Chen, L. Zheng, Q. Lu, X. Yang, R. Xu, T. Xiao, J. Li, D. Wang, Q. Peng, C. Chen, Y. Li, Nat. Chem. '01.', 11, 222.
- [65] Z. Lu, B. Wang, Y. Hu, W. Liu, Y. Zhao, R. Yang, Z. Li, J. Luo, B. Chi, Z. Jiang, M. Li, S. Mu, S. Liao, J. Zhang, X. Sun, Angew. Chem., Int. Ed. 2019, 58, 2622.
- [66] J. P. Perdew, K. Burke, M. Ernzerhof, Phys. Rev. Lett. 1996, 77, 3865.
- [67] P. E. Blöchl, Phys. Rev. B 1994, 50, 17953.
- [68] G. Kresse, J. Furthmüller, Phys. Rev. B 1996, 54, 11169.
- [69] H. J. Monkhorst, J. D. Pack, Phys. Rev. B 1976, 13, 5188.
- [70] G. Henkelman, B. P. Uberuaga, H. Jónsson, J. Chem. Phys. 2000, 113, 9901.
- [71] G. Henkelman, A. Arnaldsson, H. Jonsson, Comput. Mater. Sci. 2006, 36, 354.

